

# Quantum interference with independent single-photon sources over 300 km fiber

Xiang You,<sup>a,b,c,†</sup> Ming-Yang Zheng,<sup>d,†</sup> Si Chen,<sup>b,c,†</sup> Run-Ze Liu,<sup>b,c,†</sup> Jian Qin,<sup>b,c</sup> Mo-Chi Xu,<sup>b,c</sup> Zheng-Xuan Ge,<sup>b,c</sup> Tung-Hsun Chung,<sup>b,c</sup> Yu-Kun Qiao,<sup>b,c</sup> Yang-Fan Jiang,<sup>d</sup> Han-Sen Zhong,<sup>b,c</sup> Ming-Cheng Chen,<sup>b,c</sup> Hui Wang,<sup>b,c</sup> Yu-Ming He,<sup>b,c</sup> Xiu-Ping Xie,<sup>d</sup> Hao Li,<sup>e</sup> Li-Xing You,<sup>g</sup> Christian Schneider,<sup>f,g</sup> Juan Yin,<sup>b,c</sup> Teng-Yun Chen,<sup>b,c</sup> Mohamed Benyoucef,<sup>h</sup> Yong-Heng Huo,<sup>b,c</sup> Sven Höfling,<sup>f</sup> Qiang Zhang,<sup>b,c,d</sup> Chao-Yang Lu,<sup>b,c,i,\*</sup> and Jian-Wei Pan<sup>b,c,\*</sup>

<sup>a</sup>University of Science and Technology of China, School of Cyberspace Security, Hefei, China

<sup>b</sup>University of Science and Technology of China, Hefei National Laboratory for Physical Sciences at Microscale, Department of Modern Physics, Hefei, China

<sup>c</sup>University of Science and Technology of China, CAS Centre for Excellence in Quantum Information and Quantum Physics, Shanghai, China

<sup>d</sup>Jinan Institute of Quantum Technology, Jinan, China

<sup>e</sup>Chinese Academy of Sciences, Shanghai Institute of Microsystem and Information Technology (SIMIT), State Key Laboratory of Functional Materials for Informatics, Shanghai, China

<sup>f</sup>Universität Würzburg, Technische Physik, Physikalisches Institut and Wilhelm Conrad Röntgen-Center for Complex Material Systems, Würzburg, Germany

<sup>g</sup>University of Oldenburg, Institute of Physics, Oldenburg, Germany

<sup>h</sup>University of Kassel, Institute of Nanostructure Technologies and Analytics, CINSaT, Kassel, Germany

<sup>i</sup>NYU-ECNU Institute of Physics at NYU Shanghai, Shanghai, China

**Abstract.** In the quest to realize a scalable quantum network, semiconductor quantum dots (QDs) offer distinct advantages, including high single-photon efficiency and indistinguishability, high repetition rate (tens of gigahertz with Purcell enhancement), interconnectivity with spin qubits, and a scalable on-chip platform. However, in the past two decades, the visibility of quantum interference between independent QDs rarely went beyond the classical limit of 50%, and the distances were limited from a few meters to kilometers. Here, we report quantum interference between two single photons from independent QDs separated by a 302 km optical fiber. The single photons are generated from resonantly driven single QDs deterministically coupled to microcavities. Quantum frequency conversions are used to eliminate the QD inhomogeneity and shift the emission wavelength to the telecommunication band. The observed interference visibility is  $0.67 \pm 0.02$  ( $0.93 \pm 0.04$ ) without (with) temporal filtering. Feasible improvements can further extend the distance to  $\sim 600$  km. Our work represents a key step to long-distance solid-state quantum networks.

Keywords: quantum networks; quantum dots; solid-state single-photon sources; quantum frequency conversion; quantum interference.

Received Nov. 19, 2022; accepted for publication Nov. 24, 2022; published online Dec. 27, 2022.

© The Authors. Published by SPIE and CLP under a Creative Commons Attribution 4.0 International License. Distribution or reproduction of this work in whole or in part requires full attribution of the original publication, including its DOI.

[DOI: [10.1117/1.AP.4.6.066003](https://doi.org/10.1117/1.AP.4.6.066003)]

## 1 Introduction

Quantum communications exploit the fundamental properties of quantum mechanics, such as superposition and entanglement, to implement communication tasks that are infeasible with classical means. Examples include quantum key distribution<sup>1,2</sup>

and quantum teleportation.<sup>3</sup> Since the early days of table top experiments,<sup>4,5</sup> one of the most significant challenges of the field is to extend the distance of quantum communication to a practically useful scale. Exciting progress<sup>6</sup> has been made over the past decades that culminated in satellite-based quantum communication over 1000 km.<sup>7</sup> Taking advantage of the empty outer space, the satellite-based transmission channel showed a much lower loss than the optical fibers.

In addition to the quantum channel, another important ingredient of long-distance quantum communications is the quantum

\*Address all correspondence to Chao-Yang Lu, [cylu@ustc.edu.cn](mailto:cylu@ustc.edu.cn); Jian-Wei Pan, [pan@ustc.edu.cn](mailto:pan@ustc.edu.cn)

<sup>†</sup>These authors contributed equally to this work.

light source.<sup>8,9</sup> An ideal candidate is a single-photon source that emits one and only one photon each time.<sup>10</sup> To obtain a high count rate after transmission, the single-photon sources should have a high system efficiency (which includes the generation,<sup>11</sup> extraction,<sup>12,13</sup> and collection<sup>14</sup> efficiencies) and high repetition rate<sup>15,16</sup> (which is intrinsically limited by the emitter's radiative lifetime). For quantum network applications, such as quantum teleportation, which requires interfering independent photons, the single photons should be transform-limited.<sup>17</sup> Additional requirements include a scalable platform, tunable and narrow-band linewidth (favorable for temporal synchronization), and interconnectivity with matter qubits. Quantum dots (QDs) have been considered a promising solid-state system for quantum networks.<sup>9,10,17,18</sup> However, previous attempts at QD-based two-photon interferences<sup>19–29</sup> were limited to a few kilometer scales. There are a number of challenges to achieve a long-distance quantum interference, including high performance on single-photon source brightness, purity, indistinguishability, wavelength band and matching, high-fidelity transmission, and more crucially, integrating all these parameters together compatibly.

In this article, we report high-visibility quantum interference between two independent QDs linked with ~300 km optical fibers by developing efficient and indistinguishable single-photon sources, ultralow noise and tunable single-photon frequency conversion, and low-dispersion long fiber transmission. As a first step, our experiment points to a promising route to long-distance solid-state quantum networks.<sup>9</sup>

## 2 Single-Photon Sources

Our experimental configuration is shown in Fig. 1. Two QDs are housed inside two cryogenic-free cryostats with a temperature

of 4 and 1.7 K, respectively. To maximize the efficiency and indistinguishability of the single photons, the QDs are spectrally and spatially optimally coupled to microcavities. Two different types of microcavities are used: QD1 is embedded inside a narrowband micropillar, and QD2 is coupled to a broadband bullseye cavity. Under resonant  $\pi$ -pulse excitation by an ultrafast laser, resonance fluorescence single photons at wavelengths of  $\lambda_{\text{QD1}} = 893.16$  nm ( $\lambda_{\text{QD2}} = 891.92$  nm) are emitted from QD1 (QD2) and collected into single-mode fibers.

Under an 80.3-MHz pumping rate, at the output of collection single-mode optical fibers, the final single-photon rate is 20.2 and 16.2 MHz for QD1 and QD2, respectively, corresponding to a system efficiency of 25% and 20%. The second-order correlations of the single-photon sources are characterized by Hanbury–Brown–Twiss (HBT) measurements, which give  $g_{\text{QD1}}^{(2)}(0) = 0.072(1)$  and  $g_{\text{QD2}}^{(2)}(0) = 0.051(1)$ , as plotted in Fig. 2(a). The mutual indistinguishability between two single photons from the same QDs is measured using a Hong–Ou–Mandel (HOM) interferometer where they overlap at a 50:50 beam splitter. These two single photons are consecutively emitted from the same QDs with a time separation of 12.5 ns. Figure 2(b) shows the histograms of normalized coincidences for the two photons set at parallel and orthogonal polarizations. After correction of the residual second-order correlation, we extract a photon indistinguishability of 91.9(1)% and 83.9(3)% for QD1 and QD2, respectively.

It is important to note the difference between the mutual indistinguishability at 12.5-ns separation and the Fourier transform limit.<sup>17</sup> The former is immune to any environmentally induced spectral diffusion that occurs at a time scale much slower than 12.5 ns. What really matters for the quantum

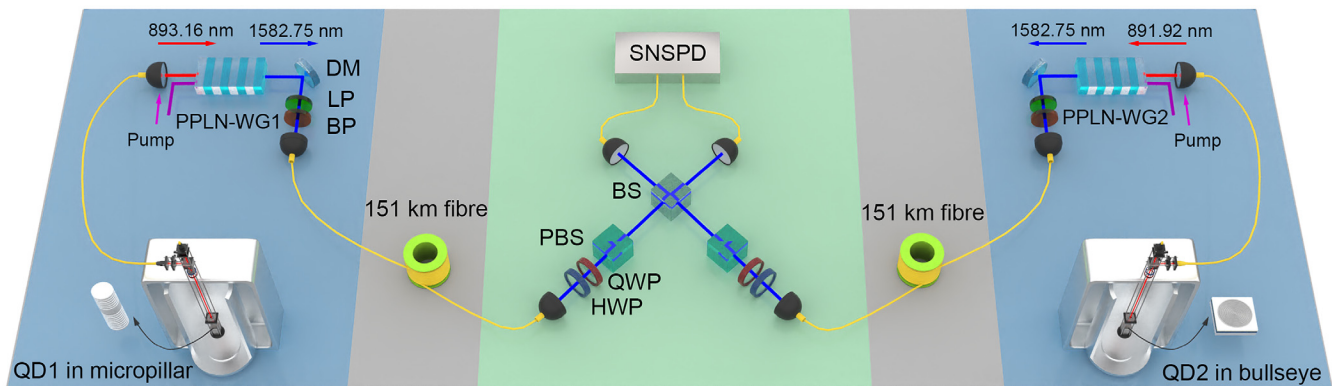


**Fig. 1** Experimental configuration of quantum interference between two independent solid-state QD single-photon sources separated by 302 km fiber. Both QDs are embedded in microcavities, with QD1 in a micropillar and QD2 in a bullseye cavity. Under resonant  $\pi$ -pulse excitation (not shown), the single photons are emitted from QD1 (QD2), collected by a confocal setup, and then sent into QFC1 (QFC2), which consists of PPLN-WG, pump lasers (not shown, with different wavelengths), and filters (DM, dichromatic mirror; LP, long pass; BP, bandpass). The wavelength of single photons from QD1 (QD2) is converted from near-infrared to 1582.75 nm in QFC1 (QFC2) by adjusting the wavelengths of the pump lasers. The downconverted photons both transmit through 151 km optical fiber and impinge upon a 50:50 beam-splitter (BS) via HOM interference. Arrivals of single photons after interference are detected by two superconducting nanowire single-photon detectors (SNSPDs) and then analyzed using a time-to-digital converter (not shown). The emissions of single photons from QD1 and QD2 are temporally synchronized by pumping with the same laser. The combination of an HWP, a QWP, and a polarization BS makes sure the two single photons will have the same polarization during interference. All fibers are single mode to transform photons into the fundamental transverse Gaussian mode for good spatial-mode overlap.

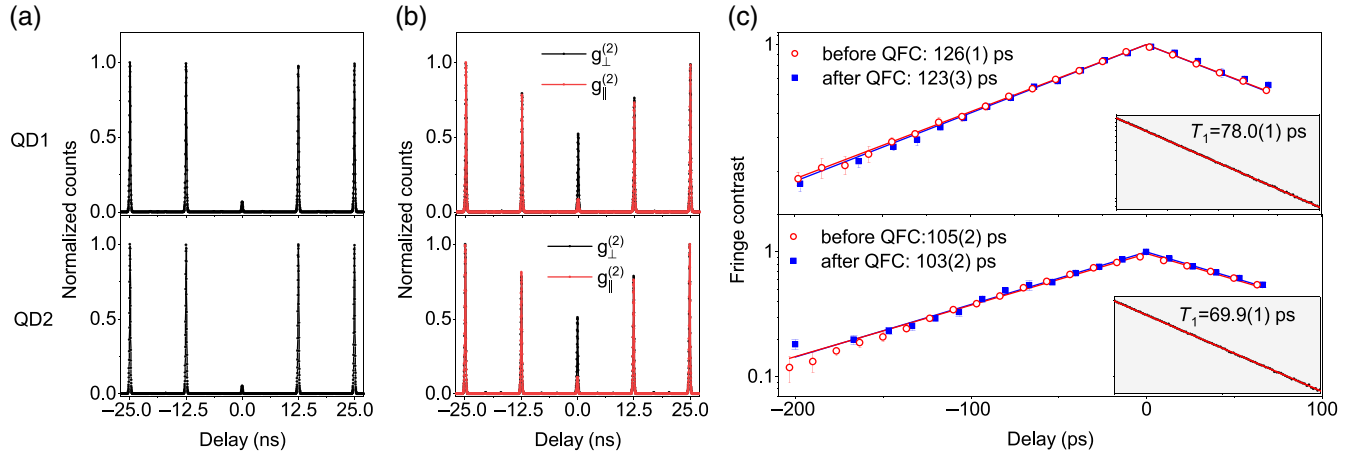


**Fig. 2** Characterization of single photons emitted from QD1 and QD2, respectively. (a) Single photon purity, HBT measurements give  $g_{\text{QD1}}^{(2)}(0) = 0.072(1)$  and  $g_{\text{QD2}}^{(2)}(0) = 0.051(1)$ . (b) Indistinguishability, HOM measurements give calculated indistinguishability of 91.9(1)% for QD1 and 83.9(3)% for QD2 after correction. The red (black) data are normalized coincidence counts for two polarizing parallel (orthogonal) photons. (c) Coherence time, measurements are carried out using a Mach–Zehnder interferometer both before QFC1 (QFC2) and after QFC1 (QFC2). By fitting the fringe contrast as temporal delay, we get extracted coherence time of 126(1) [105(2)] ps and 123(3) [103(2)] ps at different positions for QD1 (QD2). The insets show the corresponding single-photon radiative lifetimes for QD1 and QD2, which are calculated by fitting the one-sided exponential decay.

interference between independent QDs is the degree of transform limit, that is, the ratio of  $T_2/2T_1$ , where  $T_1$  and  $T_2$  are radiative lifetime and coherent time of the single photons, respectively. We measure  $T_1$  using time-resolved pulsed resonance fluorescence. By fitting the exponential decay, we extract the radiative lifetime  $T_1$  of 78.0(1) ps for QD1 and 69.9(1) ps for QD2, as illustrated in the insets of Fig. 2(c). The coherence time is measured using a Mach–Zehnder interferometer and then calculated by fitting the fringe contrast as a function of temporal delay. Figure 2(c) shows the coherence time of the single photons, which is 126(1) ps for QD1 and 105(2) ps for QD2. These allow us to calculate the degree of transform limit as 80.8(1)% for QD1 and 75.1(1)% for QD2, which are slightly lower than the 12.5-ns indistinguishability we expected.

### 3 Quantum Frequency Conversion

There are two main challenges in sending the QD single photons through long-distance optical fibers and observing quantum interference. First, the InAs QDs emission is at a wavelength of  $\sim 890$  nm, which should be converted to telecommunication wavelength to exploit the low transmission loss in commercially available fibers. So far, the QDs directly emitting single photons in the telecommunications wavelength<sup>30–34</sup> have not yet reached a photon count rate comparable to their near-infrared counterparts. Second, the self-assembled QDs emit single photons intrinsically at different wavelengths, which would reveal which-way information to prevent the HOM interference.

In this work, we use quantum frequency conversion (QFC)<sup>35–37</sup> to overcome both problems. To this end, we fabricate a periodically poled lithium niobate (PPLN) waveguide for difference frequency generation (see Fig. S3 in the Supplemental Material). The energy conservation demands  $1/\lambda_c = 1/\lambda_s - 1/\lambda_p$ , where  $\lambda_s$ ,  $\lambda_p$ , and  $\lambda_c$  represent the wavelengths of the signal, pump,

and converted photons, respectively. To precisely tune the two converted wavelengths into resonance, the pump lasers have both a coarse tuning range of  $\sim 1$  nm and a fine tuning resolution of 3.6 MHz using the laser piezoelectric (PZT) actuator, which is  $\sim 40$  times and  $\sim 0.1\%$  of the QD emission linewidth, respectively [Fig. 3(a)]. For the wavelengths of QD1 and QD2, the pump lasers are tuned at 2049.98 and 2043.46 nm, respectively, which converts both into 1582.75 nm (as labeled in Fig. 1).

By optimizing the nonlinear interaction, waveguide coupling, and transmission rate, the overall single-photon conversion efficiencies reach  $\sim 50\%$  for both devices [Fig. 3(b)]. To suppress the noise background from the residual pump laser, harmonic generation, and broadband Raman photons induced by the strong pump laser, we use a combination of dichromatic mirrors and optical filters to obtain a signal-to-noise ratio of 28 to 30 dB [Fig. 3(c)]. We note that an advantage of the frequency conversion process is that it does not interfere with the quantum emitter itself. To test whether the converted photons still preserve the coherence properties of the signal single photons, we measure the purity and coherence time of the single photons after conversion, which, as plotted in Fig. S4 in the Supplemental Material and Fig. 2(c), show near-perfect overlap with the data before conversion.

### 4 Fiber Transmission of Single Photons

The dominant loss is from the long-distance fiber transmission of the single photons. As the transmission rate of the fiber is 0.19 dB/km, the loss over 300 km is 57 dB. Fiber transmission of single photons not only causes photon loss, but can also influence photon's properties. For example, the orientation of photon polarization can be changed in optical fibers. The photon's arrival time can drift due to the change of the fiber length caused by temperature fluctuation.

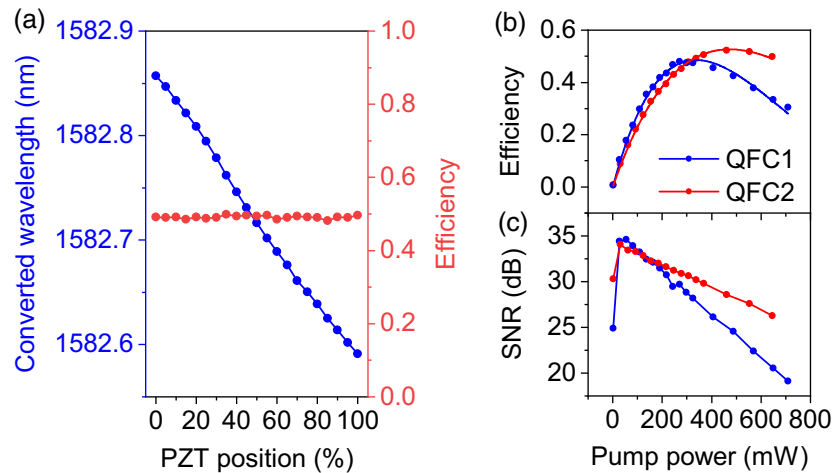


**Fig. 3** Characterization of the QFC setup. (a) Fine-tuning of the wavelength of downconverted photons as a function of the position of pump laser's PZT actuator. The tuning resolution is  $\sim 0.03$  pm, corresponding to  $\sim 3.6$  MHz in the frequency domain. The conversion efficiency is stable in the whole fine-tuning range. (b) Conversion efficiency and (c) signal-to-noise ratio as a function of pump power. The maximum end-to-end efficiency is 48% (52%) at 271 mW (461 mW) for QFC1 (QFC2). The corresponding signal-to-noise values at maximum efficiencies are 29.8 and 28.5 dB, respectively.

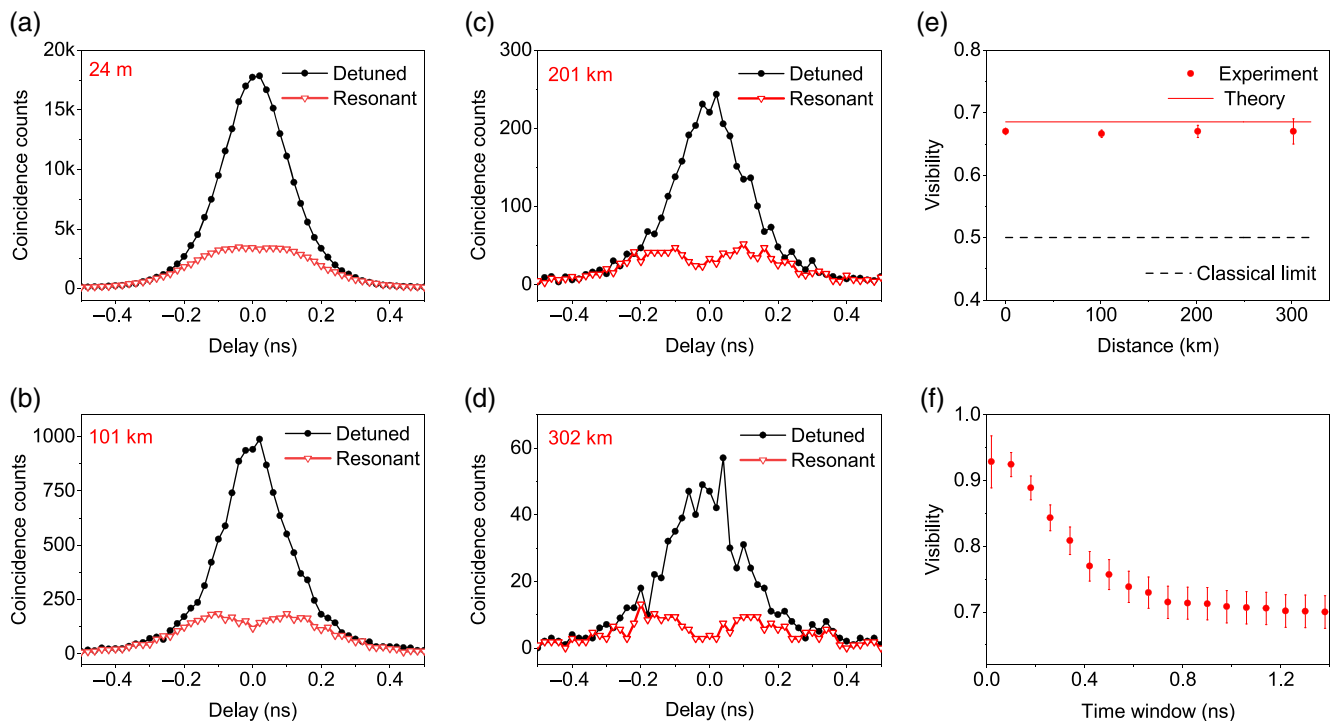


**Fig. 4** Quantum interference between two solid-state QD single photon sources. (a)–(d) Measurements of coincidence counts between two downconverted photons separated by total fiber lengths of 24 m, 101 km, 201 km, and 302 km, respectively (the 24 m is from the photon collection system before QFC). Red triangles and black dots are the two-photon coincidence counts under the same frequency and 38-GHz detuned, respectively. The integration time for the data set of (a)–(d) is 5 s, 24 s, 9 min, and 2.5 h, respectively. (e) Experimental raw visibilities and theoretical visibility (red line) as a function of fiber length. Both are well above the classical limit of 50%. (f) Dependence of raw visibility on coincidence time window with experimental data extracted from (d). The raw visibility reaches up to  $0.93 \pm 0.04$  at 20 ps.

Efforts are taken to preserve the photon's properties during the fiber transmission. To reduce the drift of the photon's arrival time, the temperature of the fibers is stabilized within  $\pm 0.1^\circ\text{C}$ . The measured typical time drift is within 10 ps per hour, which is much smaller than the photon's coherence time. A set of half-wave-plates (HWPs) and quarter-wave-plates (QWPs) is used to control the polarization. As shown in Fig. S6 in the [Supplemental Material](#), there is a slow wandering of polarization drift over hours, which is transformed into  $\sim 10\%$  level efficiency loss by applying polarization filtering at the end of the optical fibers.

There is also an effect of frequency dispersion in optical fibers owing to a wavelength-dependent velocity, which could reduce the indistinguishability of the single photons. The dispersions of QD1 and QD2 single photons over the 150-km fiber are 66.5 and 89.4 ps, respectively, which are comparable to the single photon's coherence time of 105 to 120 ps. If two photons go through the same fiber length, they will experience the same dispersion. The symmetric transmission configuration setup in our experiment thus makes the two-photon interference immune to fiber dispersion.<sup>38,39</sup>

## 5 Remote Two-Photon Interference

After faithful transmission over the optical fibers, the two single photons in the outputs are synchronized and superposed on a beam splitter for quantum interference. We use superconducting nanowire single-photon detectors with an efficiency of 76% and a time resolution of  $\sim 70$  ps to register the finally arrived photons. The two-photon coincidence counts when the two photons are controllably set at the same frequency (red) and far-detuned (black,  $\Delta\nu = 38$  GHz) are plotted for a range of total fiber length of 24 m [Fig. 4(a)], 101 km [Fig. 4(b)], 201 km [Fig. 4(c)], and 302 km [Fig. 4(d)]. Note that the

counts presented here are the raw data without any background subtraction.

The extracted raw visibilities are at a level of  $0.67 \pm 0.02$  for different optical fiber lengths. There is no evident drop in the visibility for increasing fiber length, as expected from the dispersion-cancellation symmetric transmission. These raw visibilities significantly exceed the classical limit of 50%, which conclusively demonstrates genuine two-photon quantum interference. The visibilities are plotted (red dots) in Fig. 4(e) as a function of the fiber length, which is in good agreement with the theoretical calculation (red line) that considers the  $T_2/2T_1$  for each QD, their bandwidth mismatch, and their imperfect second-order correlations. Considering the  $g_{\text{QD1}}^{(2)}(0)$  and  $g_{\text{QD2}}^{(2)}(0)$ , the corrected two-photon interference visibility is  $0.73 \pm 0.02$  at 302 km.

Temporal filtering can also significantly increase the two-photon interference visibility. The time resolution of the single-photon detectors is 70 ps, much smaller than a photon's coherence time. We plot in Fig. 4(f) the raw visibilities as a function of coincidence time window. The raw visibility increases substantially with a narrowing time window, as the temporal filtering effectively improves the coherence of the single photons. At 20 ps, the visibility reaches  $0.93 \pm 0.04$ . Note that such a filtering, only at the cost of heralding efficiency, can be useful in future experiments on high-fidelity entanglement swapping of single photons<sup>40,41</sup> and single spins.<sup>42,43</sup>

## 6 Future

Figure 5(a) summarizes two-photon interference distance and visibilities of previously reported work between two QDs, to the best of our knowledge.<sup>19–29</sup> This experiment establishes a distance that is more than 2 orders of magnitude larger than the previous record, with, simultaneously, the highest visibility.

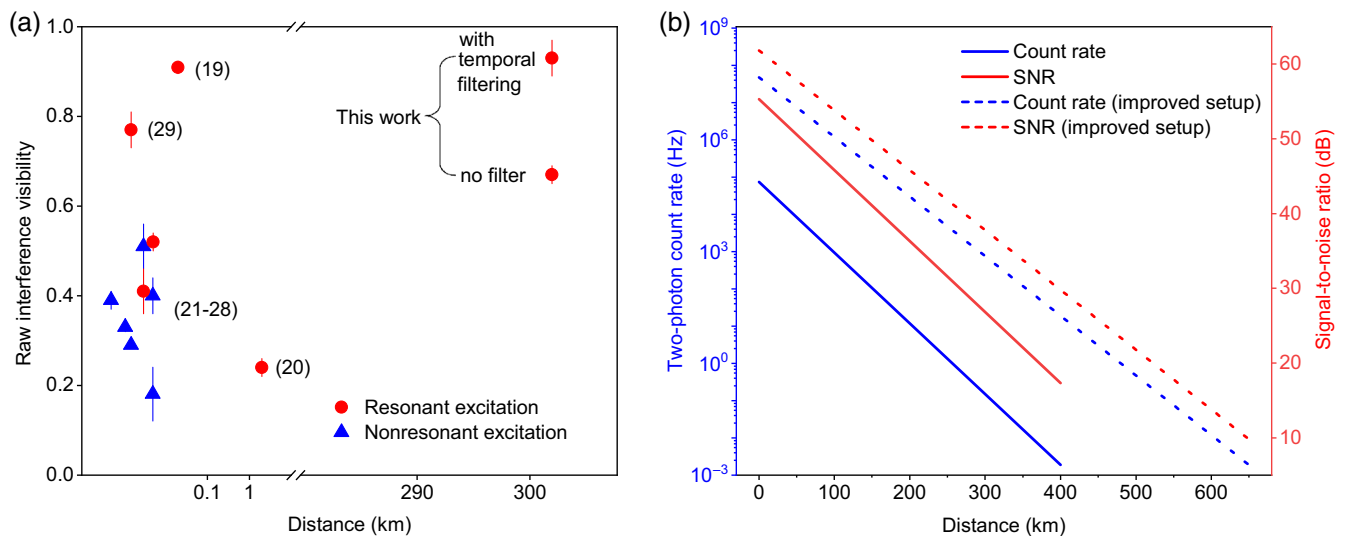


**Fig. 5** Summary of previously reported work and outlook. (a) Summary of quantum interference visibilities between two solid-state QD single-photon sources as a function of distance. (b) Simulations of two-photon coincidence count rate and signal-to-noise ratio as a function of optical fiber length with different system parameters. The solid lines are simulated with parameters of this experiment, including  $\nu_{\text{pulse}} = 80$  MHz (repetition rate of pulsed excitation laser),  $\eta_{\text{sys}} = 0.2$  (photon system efficiency),  $n_{\text{dc}} = 300$  Hz (dark counts of SNSPD), and  $\eta_{\text{loss}} = 0.19$  dB/km (loss of optical fiber). The dotted lines are simulated with feasibly improved parameters of  $\nu_{\text{pulse}} = 2.6$  GHz,  $\eta_{\text{sys}} = 0.8$ , and  $\eta_{\text{loss}} = 0.16$  dB/km.

A number of straightforward improvements can further extend the distances. The short  $T_1$  of the QDs enabled by the high Purcell factors allows one to increase the repetition rate from 80 MHz to 2.6 GHz, a  $\sim 30$  times enhancement. Using tunable open microcavities,<sup>16</sup> it is feasible for the single photon system efficiency to reach 80%. In addition, ultralow-loss optical fiber with transmission loss of 0.16 dB/km has become available. A numerical simulation curve is plotted in Fig. 5(b). With these ready improvements, the transmission distance can be extended to  $\sim 600$  km, where the coincidence count rate will be 0.012 Hz with a signal-to-noise ratio of 10 dB. Such a distance scale is already comparable to the well-developed twin-field quantum key distribution experiments.<sup>44,45</sup>

In summary, our work represents an important step toward quantum telecommunication networks using semiconductor QDs and telecom fiber channels. The experiment creates a solid-state platform to implement quantum teleportation,<sup>5</sup> entanglement swapping,<sup>40,41</sup> quantum relay,<sup>46</sup> and teleportation of controlled NOT gates at hundreds of kilometers scale in a multi-user network configuration. A key advantage of using the single QDs, compared to spontaneous parametric downconversion, is the intrinsically deterministic single-photon emission and natural suppression of double pair events, which can allow the realization of multi-photon entanglement and interferometry in a non-postselection way.<sup>6</sup> A large number of entangled photons can be generated in this platform by, e.g., heralded creation of three-photon Greenberger–Horne–Zeilinger states<sup>47</sup> from six single photons, and using it as a basic resource and fuse into larger ones,<sup>48</sup> which will be useful resources for all-photonic quantum repeaters<sup>49</sup> and distributed quantum computing. The distances and functionalities can be further improved by combining with suitable quantum memories. Thus, intercity-scale fully quantum networks appear technologically promising based on a scalable semiconductor platform.

**Note:** See [Supplemental Material](#) for theoretical analysis of two-photon quantum interference and more detailed descriptions for quantum-dot single-photon sources and QFC, which includes Refs. 50–53.

## Acknowledgments

This work was supported by the National Natural Science Foundation of China (91836303), the National Key R&D Program of China (2019YFA0308700), the Chinese Academy of Sciences, the Anhui Initiative in Quantum Information Technologies, the Natural Science Foundation of Shandong Province (ZR2020LLZ007), and the Shanghai Municipal Science and Technology Major Project (2019SHZDZX01).

## References

1. C. H. Bennett and G. Brassard, "Quantum cryptography: public key distribution and coin tossing," in *Proc. IEEE Int. Conf. Comput. Syst. Signal Process.*, Vol. 175, p. 8 (1984).
2. A. K. Ekert, "Quantum cryptography based on Bell's theorem," *Phys. Rev. Lett.* **67**(6), 661–663 (1991).
3. C. H. Bennett et al., "Teleporting an unknown quantum state via dual classical and Einstein-Podolsky-Rosen channels," *Phys. Rev. Lett.* **70**(13), 1895–1899 (1993).
4. C. H. Bennett and G. Brassard, "Experimental quantum cryptography: the dawn of a new era for quantum cryptography: the experimental prototype is working," *ACM Sigact News* **20**(4), 78–80 (1989).
5. D. Bouwmeester et al., "Experimental quantum teleportation," *Nature* **390**(6660), 575–579 (1997).
6. J.-W. Pan et al., "Multiphoton entanglement and interferometry," *Rev. Mod. Phys.* **84**(2), 777–838 (2012).
7. C.-Y. Lu et al., "Micius quantum experiments in space," *Rev. Mod. Phys.* **94**(3), 035001 (2022).
8. N. Gisin et al., "Quantum cryptography," *Rev. Mod. Phys.* **74**(1), 145–195 (2002).
9. C.-Y. Lu and J.-W. Pan, "Quantum-dot single-photon sources for the quantum Internet," *Nat. Nanotechnol.* **16**(12), 1294–1296 (2021).
10. P. Senellart, G. Solomon, and A. White, "High-performance semiconductor quantum-dot single-photon sources," *Nat. Nanotechnol.* **12**(11), 1026–1039 (2017).
11. Y.-M. He et al., "On-demand semiconductor single-photon source with near-unity indistinguishability," *Nat. Nanotechnol.* **8**(3), 213–217 (2013).
12. X. Ding et al., "On-demand single photons with high extraction efficiency and near-unity indistinguishability from a resonantly driven quantum dot in a micropillar," *Phys. Rev. Lett.* **116**(2), 020401 (2016).
13. N. Somaschi et al., "Near-optimal single-photon sources in the solid state," *Nat. Photonics* **10**(5), 340–345 (2016).
14. H. Wang et al., "Towards optimal single-photon sources from polarized microcavities," *Nat. Photonics* **13**(11), 770–775 (2019).
15. F. Liu et al., "High Purcell factor generation of indistinguishable on-chip single photons," *Nat. Nanotechnol.* **13**(9), 835–840 (2018).
16. N. Tomm et al., "A bright and fast source of coherent single photons," *Nat. Nanotechnol.* **16**(4), 399–403 (2021).
17. H. Wang et al., "Near-transform-limited single photons from an efficient solid-state quantum emitter," *Phys. Rev. Lett.* **116**(21), 213601 (2016).
18. P. Lodahl, "Quantum-dot based photonic quantum networks," *Quantum Sci. Technol.* **3**(1), 013001 (2017).
19. L. Zhai et al., "Quantum interference of identical photons from remote GaAs quantum dots," *Nat. Nanotechnol.* **17**(8), 829–833 (2022).
20. J. H. Weber et al., "Two-photon interference in the telecom C-band after frequency conversion of photons from remote quantum emitters," *Nat. Nanotechnol.* **14**(1), 23–26 (2019).
21. M. Zopf et al., "Frequency feedback for two-photon interference from separate quantum dots," *Phys. Rev. B* **98**(16), 161302 (2018).
22. A. Thoma et al., "Two-photon interference from remote deterministic quantum dot microlenses," *Appl. Phys. Lett.* **110**(1), 011104 (2017).
23. M. Reindl et al., "Phonon-assisted two-photon interference from remote quantum emitters," *Nano Lett.* **17**(7), 4090–4095 (2017).
24. V. Giesz et al., "Cavity-enhanced two-photon interference using remote quantum dot sources," *Phys. Rev. B* **92**(16), 161302 (2015).
25. P. Gold et al., "Two-photon interference from remote quantum dots with inhomogeneously broadened linewidths," *Phys. Rev. B* **89**(3), 035313 (2014).
26. R. B. Patel et al., "Two-photon interference of the emission from electrically tunable remote quantum dots," *Nat. Photonics* **4**(9), 632–635 (2010).
27. S. Ates et al., "Two-photon interference using background-free quantum frequency conversion of single photons emitted by an InAs quantum dot," *Phys. Rev. Lett.* **109**(14), 147405 (2012).
28. E. B. Flagg et al., "Interference of single photons from two separate semiconductor quantum dots," *Phys. Rev. Lett.* **104**(13), 137401 (2010).
29. Y. He et al., "Indistinguishable tunable single photons emitted by spin-flip Raman transitions in InGaAs quantum dots," *Phys. Rev. Lett.* **111**(23), 237403 (2013).
30. L. Seravalli et al., "Single quantum dot emission at telecom wavelengths from metamorphic InAs/InGaAs nanostructures

- grown on GaAs substrates,” *Appl. Phys. Lett.* **98**(17), 173112 (2011).
31. T. Miyazawa et al., “Single-photon emission at 1.5  $\mu\text{m}$  from an InAs/InP quantum dot with highly suppressed multi-photon emission probabilities,” *Appl. Phys. Lett.* **109**(13), 132106 (2016).
  32. J.-H. Kim et al., “Two-photon interference from a bright single-photon source at telecom wavelengths,” *Optica* **3**(6), 577–584 (2016).
  33. M. Benyoucef et al., “Telecom-wavelength (1.5  $\mu\text{m}$ ) single-photon emission from InP-based quantum dots,” *Appl. Phys. Lett.* **103**(16), 162101 (2013).
  34. C. Nawrath et al., “Coherence and indistinguishability of highly pure single photons from non-resonantly and resonantly excited telecom C-band quantum dots,” *Appl. Phys. Lett.* **115**(2), 023103 (2019).
  35. S. Zaske et al., “Visible-to-telecom quantum frequency conversion of light from a single quantum emitter,” *Phys. Rev. Lett.* **109**(14), 147404 (2012).
  36. B. Kambs et al., “Low-noise quantum frequency down-conversion of indistinguishable photons,” *Opt. Express* **24**(19), 22250–22260 (2016).
  37. J. S. Pelc et al., “Downconversion quantum interface for a single quantum dot spin and 1550-nm single-photon channel,” *Opt. Express* **20**(25), 27510–27519 (2012).
  38. Y.-R. Fan et al., “Effect of dispersion on indistinguishability between single-photon wave-packets,” *Photonics Res.* **9**(6), 1134–1143 (2021).
  39. D.-G. Im, Y. Kim, and Y.-H. Kim, “Dispersion cancellation in a quantum interferometer with independent single photons,” *Opt. Express* **29**(2), 2348–2363 (2021).
  40. M. Zopf et al., “Entanglement swapping with semiconductor-generated photons violates Bell’s inequality,” *Phys. Rev. Lett.* **123**(16), 160502 (2019).
  41. F. B. Basset et al., “Entanglement swapping with photons generated on demand by a quantum dot,” *Phys. Rev. Lett.* **123**(16), 160501 (2019).
  42. A. Delteil et al., “Generation of heralded entanglement between distant hole spins,” *Nat. Phys.* **12**(3), 218–223 (2016).
  43. R. Stockill et al., “Phase-tuned entangled state generation between distant spin qubits,” *Phys. Rev. Lett.* **119**(1), 010503 (2017).
  44. J.-P. Chen et al., “Sending-or-not-sending with independent lasers: secure twin-field quantum key distribution over 509 km,” *Phys. Rev. Lett.* **124**(7), 070501 (2020).
  45. M. Pittaluga et al., “600-km repeater-like quantum communications with dual-band stabilization,” *Nat. Photonics* **15**(7), 530–535 (2021).
  46. H. De Riedmatten et al., “Long distance quantum teleportation in a quantum relay configuration,” *Phys. Rev. Lett.* **92**(4), 047904 (2004).
  47. D. M. Greenberger et al., “Bell’s theorem without inequalities,” *Am. J. Phys.* **58**(12), 1131–1143 (1990).
  48. S. Bartolucci et al., “Fusion-based quantum computation,” arXiv:2101.09310 (2021).
  49. K. Azuma, K. Tamaki, and H.-K. Lo, “All-photonic quantum repeaters,” *Nat. Commun.* **6**(1), 6787 (2015).
  50. B. Kambs and C. Becher, “Limitations on the indistinguishability of photons from remote solid state sources,” *New J. Phys.* **20**(11), 115003 (2018).
  51. A. M. Brańczyk, “Hong-Ou-Mandel interference,” arXiv:1711.00080 (2017).
  52. Y. Yu et al., “Entanglement of two quantum memories via fibres over dozens of kilometres,” *Nature* **578**(7794), 240–245 (2020).
  53. J. S. Pelc et al., “Long-wavelength-pumped upconversion single-photon detector at 1550 nm: performance and noise analysis,” *Opt. Express* **19**(22), 21445–21456 (2011).

Biographies of the authors are not available.